



Effect of Shape, Density, and an Array of Dimples on the Friction and Wear Performance of Laser Textured Bearing Steel under Dry Sliding

Manish Kumar, Vinayak Ranjan, and Rajnesh Tyagi

(Submitted September 23, 2019; Accepted: 14 April 2020; published online May 12, 2020)

The present study is directed to reveal the effect of density and shape of the dimples on the friction and wear characteristics of textured bearing steel (100Cr6) under dry sliding conditions. One untextured and four laser-textured disks of 100Cr6 steel with circular and bi-triangular dimples having 7 and 20% density, respectively, in the spiral layout were tested using a pin-on-disk unidirectional tribometer against a 100Cr6 pin having a flat surface with rounded corners under flat-on-flat configuration. The tests were carried at different speeds of 0.2, 0.6, and 1 m/s at a constant load of 15 N. The results indicate that a higher density of bi-triangular dimples had less wear and a lower coefficient of friction compared to untextured disk or disk with circular dimples, particularly at a relatively higher speed. This has been attributed to a relatively higher number of dimples in the contact zone in case of a spiral array, which increases the entrapment of more wear particles leading to a reduction in wear. The friction coefficient had a relatively higher value at a relatively lower speed but decreased at the highest speed of 1.0 m/s used in the present study. The results suggest that dimples may not be too effective under dry contact because they lose their effectiveness to trap wear debris after getting filled.

Keywords friction, laser texturing, wear, wear of steels

1. Introduction

Surface texturing, being used widely to enhance the tribological performance of a system, has been reported to be beneficial in controlling friction and wear in moving parts, especially those having conformal contacts (Ref 1–4). The contact between surfaces can be dry or lubricated. However, using lubricant is not always a viable way and hence puts limitations. The friction can be reduced appreciably by changing the design of the surfaces in contact. There have been successful applications of surface texturing in various fields, e.g., mechanical seals to enhance the lifetime of the machine elements, metal-forming processes with well-defined surface topographies to influence adhesion and diffusion, and magnetic hard disks. Dimples are preferred over protrusions due to ease of making, low wear, and low leakage in the case of seals. The implementation of surface textures on conformal contacts has been shown to (a) reduce interfacial friction and wear, (b) reduce energy loss, and (c) prolong the serving life of the components (Ref 5, 6). It has been reported that triangular- and square-shaped dimples exhibit a lower coefficient of friction. Also, the hindrance to the movement of the counter element is reduced due to hard deposition if carefully designed,

which is not possible in case of circular or other shapes due to symmetry (Ref 7). Arrays of the dimples on the surface have also been reported to play a major role in controlling friction. A spiral array has more and stable number of micro-dimples than a radial array under the same contact area, so the density of dimples becomes important. In the case of dry test, the availability of cavities helps in trapping wear debris and reducing the effective area of contact rather than pressure buildup as in case of the lubricated condition (Ref 8).

Various surface texturing techniques being used are indentation with hard materials (Ref 9, 10), ion etching (Ref 11), abrasive jet machining (Ref 12), lithography (Ref 13), and laser surface texturing (LST) (Ref 14–16). Out of these, laser texturing, which is a thermal energy-based machining process, is very quick, environmentally friendly, and creates a uniform, precise metal surface topography that cannot be produced by conventional methods (Ref 17–22). It has been reported that the contact should only be partially textured, which puts a limit on the width/diameter of the individual features. At the same time, it has also been suggested to keep a smaller ratio between the depth and the width of the features, thus limiting their depth. In general, improvements in the performance have been shown to occur mostly for width/diameter in the range of 5–600 μm , texture density in the range of 5 to 25%, a depth to diameter/width ratio from 0.05 to 0.15, and depths in the range from 1 to 15 μm (Ref 6, 23, 24). Zhang et al. (Ref 8) studied the frictional behavior of three differently shaped dimples, namely circular, square, and equilateral triangular, and reported that directionality of textures can be carefully utilized in bi-directional sliding condition.

Keeping this in view, a bi-triangular dimple with inward curved edges with sliding direction along its vertex has been considered for the present investigation. Hence, the present study is aimed at exploring the effect of dimples shape and density on the friction and wear performance of the laser-

Manish Kumar and **Rajnesh Tyagi**, Department of Mechanical Engineering, Indian Institute of Technology, Banaras Hindu University, Varanasi 221005, India; and **Vinayak Ranjan**, Department of Mechanical and Aerospace Engineering, Bennett University, Greater Noida 201310, India. Contact e-mail: Rtyagi.mec@itbhu.ac.in.

textured surface of bearing steel under dry contact. The 100Cr6 bearing steel has been used as it finds many applications in different rotating elements such as anti-friction bearings, crankshaft, and camshafts. Dimples of the circular and bi-triangular shapes having densities of 7 and 20%, respectively, were created through laser texturing and their effectiveness in reducing the friction, and wear was evaluated by carrying out dry sliding wear tests under low-load and low- to high-speed test regime, conformal contact using a pin-on-disk tribometer. The study also attempts to reveal the possible mechanisms of wear for the used densities, shape, and dimensions of dimples.

2. Experimental Details

2.1 Laser Surface Texturing

CAD models of specimens shown in Fig. 1 (a through d), corresponding to circular- and bi-triangular-shaped dimples having 7 and 20% density, respectively, for each were created using AutoCAD and saved in .dxf format, which were further used as inputs for laser surface texturing. Since the densities were already fixed, the total number of dimples was calculated using the equation $N = [(\pi D^2) \times \rho] / [\pi d^2]$, where D

is the diameter of the disk, ρ is area density and d is the diameter of the circular dimple.

Bearing steel 100Cr6 (composition 1.00% C, 0.50% Mn, 0.20% Si, 1.40% Cr) in the form of a cylindrical rod of 60 mm diameter and procured from All India Metal Corporation, Mumbai, was used as the disk material to be textured. The counterface pin was also of the same material. The disks (ϕ 50 mm and thickness 5 mm) were machined out from this rod on the lathe in the Central Workshop of IIT (BHU), Varanasi. Before texturing, the disk samples were polished using a standard metallographic procedure followed by polishing with diamond paste to attain a surface roughness of $R_a = 0.04 \mu\text{m}$. The samples were then ultrasonicated in acetone and rinsed with isopropyl alcohol. Nd:YAG fiber laser with a maximum laser power of 20 W, the wavelength of 1064 nm with one ablation, and two finishing passes was used to produce dimples of specific shape and array on the surface of steel disks by using the CAD images given in Fig. 1. Laser texturing was done at LASER JOB WORK, Noida, India. Table 1 presents the laser texturing parameters.

The textured surfaces were examined under an optical and scanning electron microscope (SEM; EVO 18, Carl Zeiss Microscope). Topographies and profiles of dimples were analyzed using a non-contact 3D optical profilometer integrated

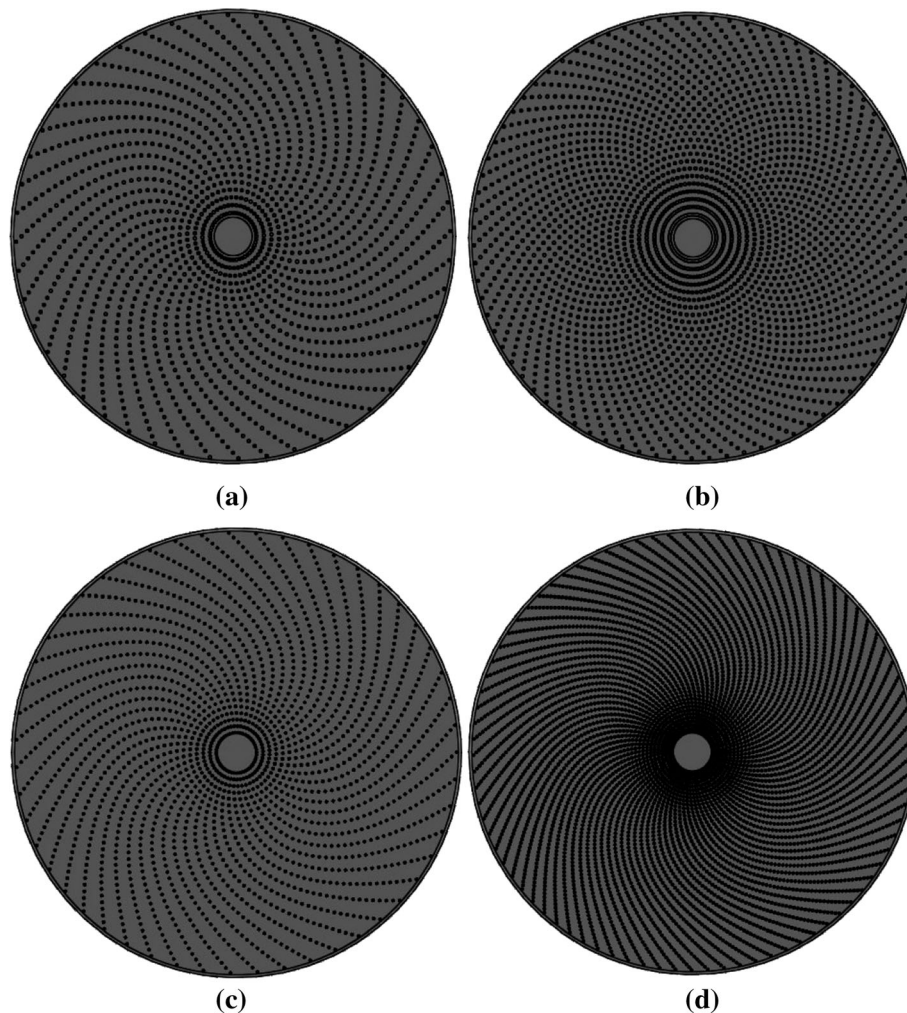


Fig. 1 CAD image of the disks textured with spiral array of (a) circular dimples, density 7%, (b) circular dimples, density 20%, (c) bi-triangular, density 7%, and (d) bi-triangular, density 20%

with a multifunctional tribometer (Rtec Instruments, USA). The inline optical 3D profilometer comes with six-objective manual or automatic turret that can accommodate several objectives and user-selectable four-color high-brightness LED light source. It has a low-noise camera unit and professional data analysis software. Each lens comes with calibration and inspection settings on the tester and an image test area with nm resolution with high-precision z-motion control. The software allows computing both line and area roughness. Calculation of nearly all ASME, ISO, and DIN surface roughness parameters can be done. Sample designations and other dimple features are given in Table 2.

2.2 Tribo-Testing

Friction and wear tests were performed on untextured and textured specimens using a rotary pin-on-disk tribometer supplied by DUCOM, Bengaluru, India, under dry sliding conditions against a pin of 100Cr6 steel having a flat face with rounded corners (Fig. 2) to have a self-mated conformal contact. Although the total number of dimples in the contact zone would be the same, for a spiral array, the number of dimples in the contact area varied from 6 to 8 and for radial pattern from 5 to 11. Hence, the spiral arrangement is expected to present a stable number of dimples. A visualization of the contact area of dimples with the counterface pin for spiral and radial arrays is depicted by a schematic diagram in Fig. 3. Both the pin and disk were polished to have an initial surface roughness of $R_a = 0.04 \mu\text{m}$. Each test was conducted with a tribo-pair, cleaned ultrasonically in acetone, and then dried. The sliding tests were conducted at a normal load of 15 N with the 5.70-mm-diameter pin for 8000 revolutions at different sliding speeds of 0.2, 0.6, and 1 m/s, respectively, under low-load and low- to medium-speed test regime. Since the tests were performed on each sample with different track radii (wear track radius 7, 12, 17, and 22 mm), the number of cycles was taken instead of time. Each test was conducted using a fresh surface of the disk and pin under atmospheric air with a room temperature of $30 \pm 2^\circ\text{C}$ and relative humidity in the range of 45-55%. Friction force was recorded in the computer through

software having an interface with the tribometer. The mass loss after a predetermined number of cycles was measured by the difference in the mass of specimens before and after the tests. An electronic weighing balance having an accuracy of 10^{-7} kg was used for measuring the mass loss, which was then converted to volume loss by dividing it with density of the specimen. Each test under a specified condition of sliding was repeated at least thrice, and the average value has been reported here. Worn surfaces of the disk were examined under SEM, and dimples were subjected to 3D optical profilometry to reveal the operative mechanisms of wear and the effect of dimple shape on the friction and wear performance.

3. Results and Discussion

3.1 Morphology of the Textured Surface

Figure 4(a through d) shows the optical micrographs of the laser-textured surfaces of the bearing steel disks with different dimple densities. A variation in the spacing between regularly formed dimples and hence, the variation in the density of dimples can be clearly observed from the figure. The spacing between the dimples along the spiral is the same in respective texturing; however, the spacing changes from one spiral to others if seen from center to circumference, as illustrated in Fig. 4(a through d).

Figure 5(a) and (c) shows the micrographs of bi-triangular and circular dimples, respectively, whereas Fig. 5(b) and (d), respectively, shows the profile of the circular and bi-triangular dimples as detected by an optical profilometer. The micro-dimples are about $500 \mu\text{m}$ in diameter and about $8 \mu\text{m}$ in depth. The metal partially gets melted due to the high-energy action of the laser, and sputtered metal gets deposited on the brim of dimples resulting in the formation of the bulge as observed from Fig. 5(c), which shows the morphology of a single dimple. The bulges on the brim of micro-dimples lead to an increase in roughness and are difficult to be completely removed by polishing.

Table 1 Laser surface texturing parameters

	Pass 1	Pass 2	Pass 3
Speed, mm/s	200	1000	1000
Power, %	80	40	30
Frequency, v	40	55	65

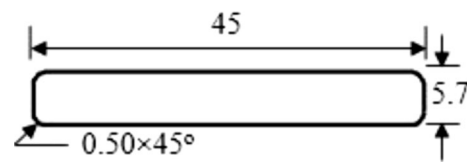


Fig. 2 Schematic diagram of counterface pin (all dimensions in mm)

Table 2 Designation of samples and topography of micro-dimples

Sample designation	Dimples	Area density	Size, dia, and side, μm	Avg, depth, μm	Distance in array, μm
UT	Untextured				
CT7	Circular	7%	500	8	1599.67
CT20	Circular	20%	500	8	714.21
BT7	Bi-triangular	7%	500 (adjacent vertices)	8	1137.51
BT20	Bi-triangular	20%	500 (adjacent vertices)	8	681.91

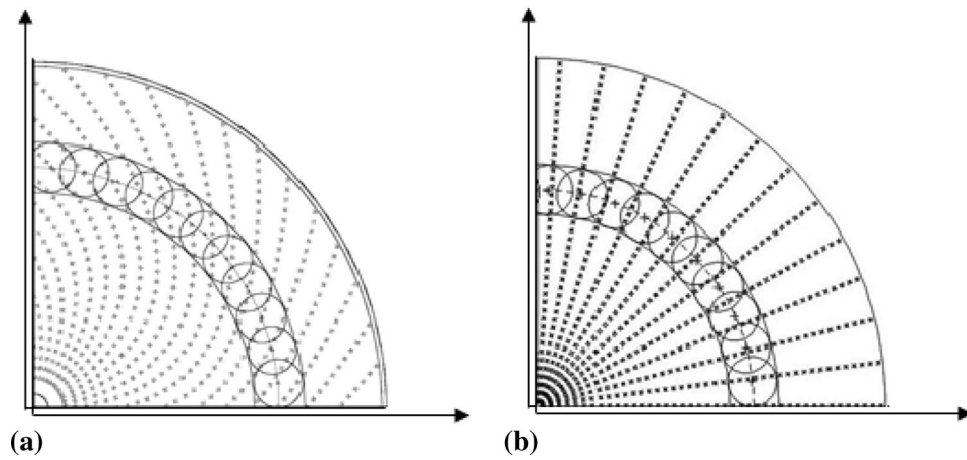


Fig. 3 Visualization of dimples in the pin contact area during disk (7% area density) rotation for spiral (a) and radial (b) arrays

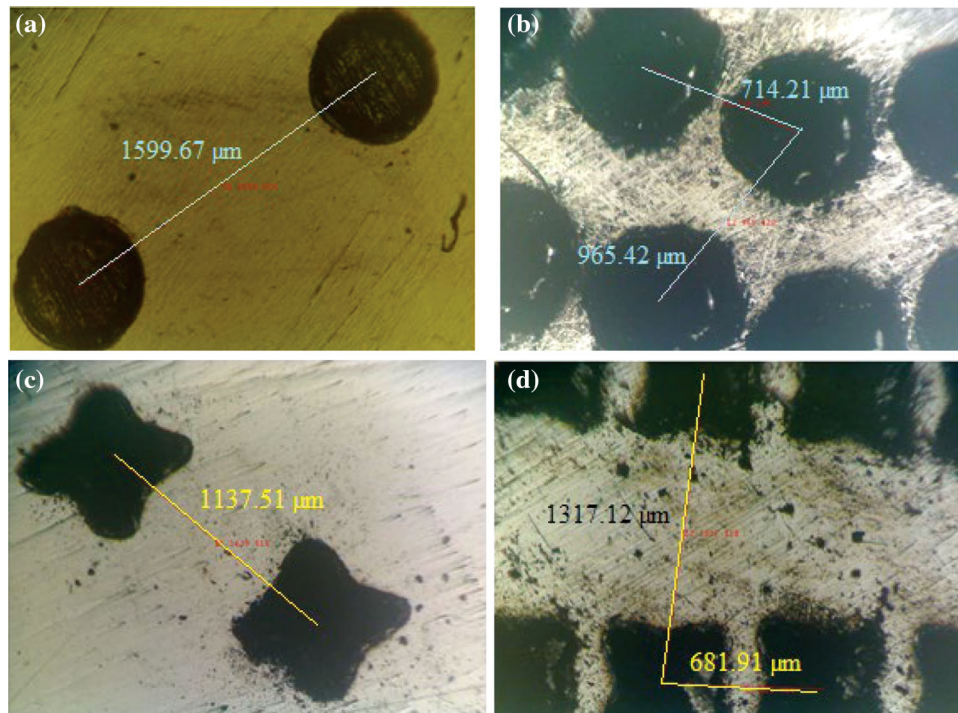


Fig. 4 Optical micrographs of laser-textured surface of steel disks having (a) 7% density of circular dimples (CT7), (b) 20% density of circular dimples (CT20), (c) 7% density of bi-triangular dimples (BT7), and (d) 20% density of bi-triangular dimples (BT20). All at 50 X (DeWinter's metallurgical microscope)

3.2 Effect of Laser Surface Texturing on the Friction and Wear Properties

Figure 6 shows the variation of the coefficient of friction with number of revolutions at 1 m/s. The variation reveals a typical fluctuating trend for all the specimens, but the amplitude of fluctuation is quite small for CT20 and BT20 in comparison with UT, CT7, and BT7. It can also be noted that the friction coefficient drops suddenly from a value of 0.6 to 0.2 for CT20 after running about 2500 cycles and maintains this value until the full duration of the test. This may be attributed to the wearing of burrs under the contact surface, leading to a smoother process of sliding.

Figure 7 shows the variation of average friction coefficient for UT, CT7, CT20, BT7, and BT20 at different sliding speeds.

The average coefficient of friction is found to be highest for 0.6 m/s speed for all the test specimens, whereas it is lowest for 0.2 m/s except for untextured (UT) and BT20. The coefficient of friction at 1.0 m/s is observed to fall in-between. However, one can observe the effect of density as well as the shape of the dimples. At the lowest speed of 0.2 m/s used in the present investigation, the friction coefficient decreases after texturing with 7% density circular dimples and remains in the same band for CT20 and BT7 before increasing finally for BT20. A similar trend of variation could be observed for a speed of 0.6 m/s, except that a decrease in friction coefficient is observed from BT7 to BT20. However, at the highest speed of 1.0 m/s, the friction coefficient first increases as one moves from untextured to CT7 before decreasing continuously as one moves from CT7

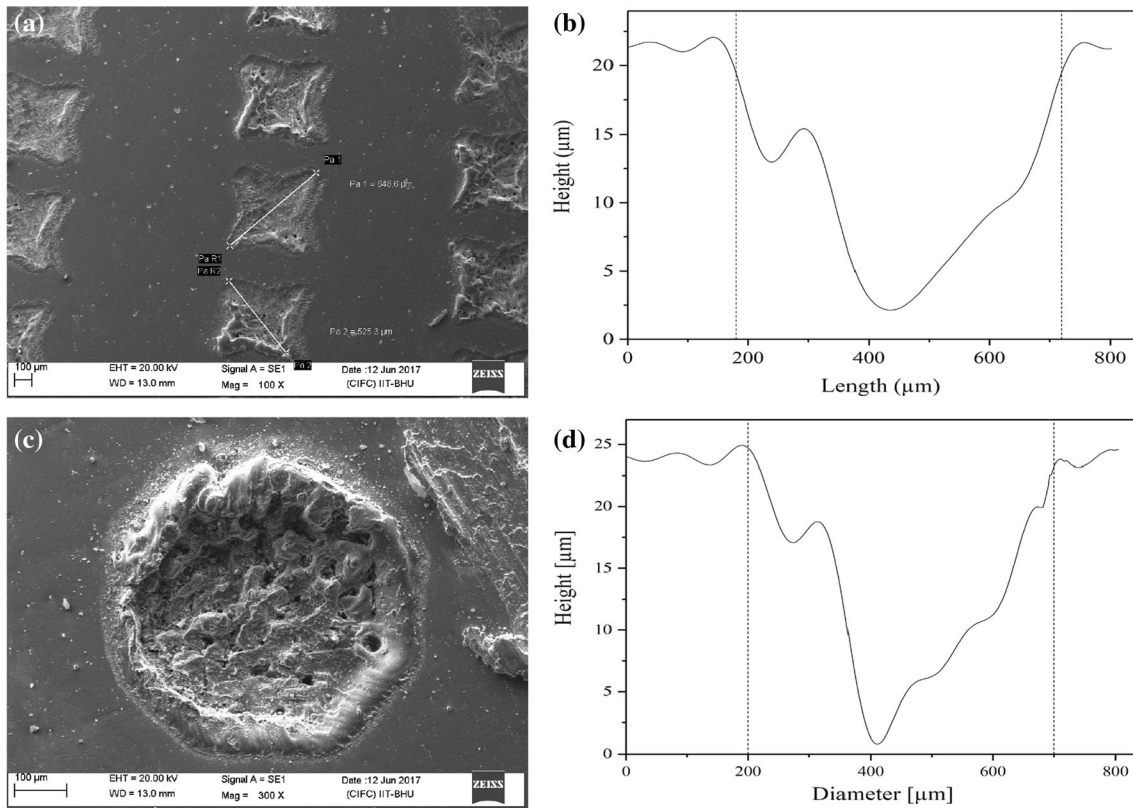


Fig. 5 SEM micrograph (a, c) and 2D profile illustrating the lengths, average depth, and height of micro-pores (b, d)

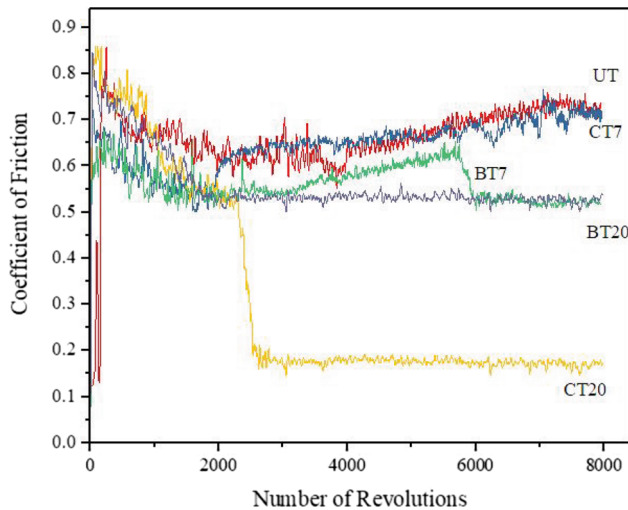


Fig. 6 Variation of friction coefficient with the number of revolutions at a speed of 1 m/s

to CT20 to BT7 to BT20, thus reflecting the effect of density as well as the shape on friction reduction.

The wear rate for each specimen has been calculated by dividing the mass loss with the density of steel (taken as $7.81 \times 10^3 \text{ kg/m}^3$). Figure 8 shows the variation of wear rate for untextured (UT) and textured specimens, namely CT7, CT20, BT7, and BT20, having different densities and shapes at various sliding speeds of 0.2, 0.6, and 1.0 m/s. One could observe that textured samples have less wear than the untextured sample at all the speeds used in the present study.

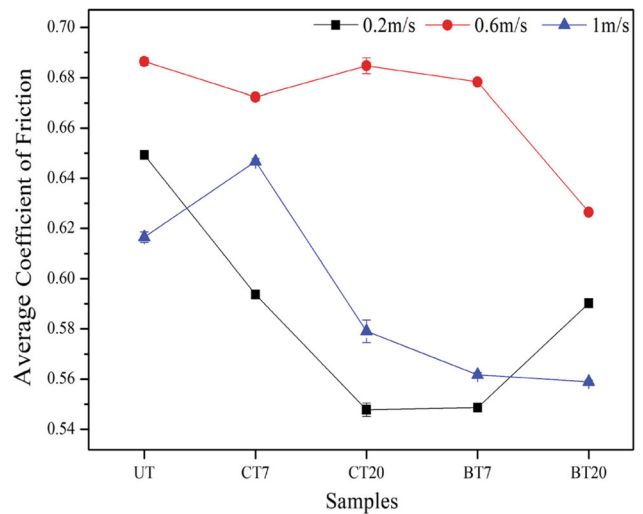


Fig. 7 Friction coefficients during sliding tests for various samples at different speeds

It can further be seen from Fig. 8 that the wear rate either decreases or remains constant as one moves from CT7 to BT7 at speeds of 0.2 and 1.0 m/s, whereas the wear rate increases from CT20 to BT7 for a speed of 0.6 m/s. The wear rate is found to decrease for speeds of 0.6 and 1.0 m/s as one moves from BT7 to BT20, whereas a slight increase could be observed for a speed of 0.2/s. The reason for more wear in the 7% circle density disk is hard deposition on the surface surrounding the cavities. The presence of microcavities entraps wear particles and minimizes wear. In the case of the untextured disk, no such

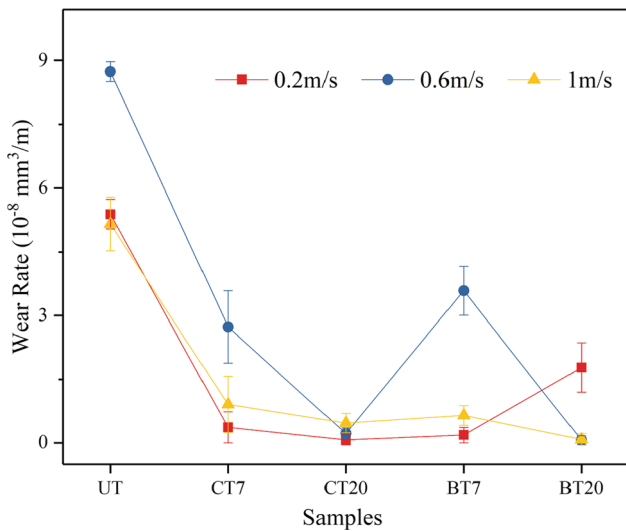


Fig. 8 Variation of wear rate in textured specimens at different speeds

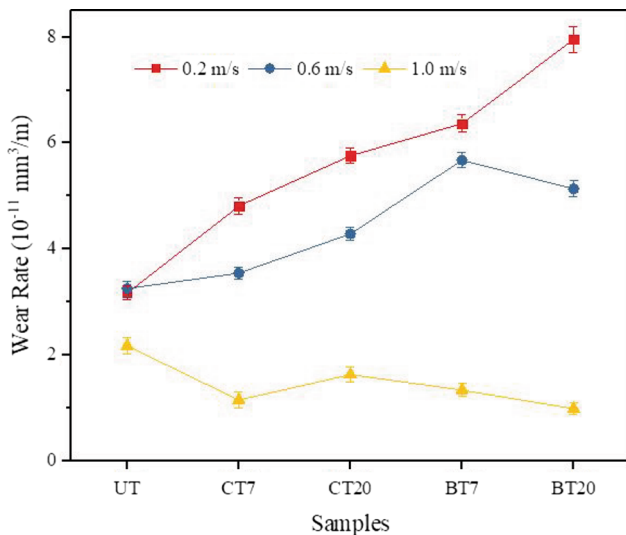


Fig. 9 Variation of wear rate in counterface pin against different samples at different speeds

feature is present, and more wear is there. More wear of textured disk with 20% bi-triangular dimples density at 0.2 m/s is because of initial presence and wear of deposition.

Figure 9 shows the variation of pin wear rate for untextured (UT) and textured specimens, namely, CT7, CT20, BT7, and BT20, at various sliding speeds of 0.2, 0.6, and 1.0 m/s. One could observe that at low-speed pin wear is more with increasing densities. It can further be seen from Fig. 9 that the wear rate decreases than that of 0.2 m/s as the speed increases to 0.6 m/s and increases as one moves from UT to BT7, whereas there is a short drop in the value for BT20. The wear rate is found to decrease significantly for speed of 1.0 m/s as one moves from UT to BT20, whereas a slight increase could be observed for CT20. The presence of hard deposition on the surface surrounding the cavities causes the pin to wear out more at 0.2 m/s. As the speed increases to 0.6 m/s, the bulge on the brim of the micro-dimple starts to wear out, which gives a

reduced value of pin wear rate. This phenomenon, however, is not observed in the case of UT. At 2.0 m/s, the bulges disappear, and the presence of an oxide layer reduces pin wear significantly.

Figure 10(a–e) shows the morphologies of textured samples as observed under a scanning electron microscope (SEM) at 0.2 m/s. The worn surface of the untextured specimen shows a typical worn morphology of steel surface with the presence of wear marks along sliding direction and signs of adhesion. The worn surfaces of textured specimens show the presence of dimples along with wear tracks running parallel to sliding direction. The dimples appear to be filled for CT7, CT20, and BT7 specimens, as seen from Fig. 10(b, c, and d), whereas the bi-triangular dimples in BT20 are yet to be filled. Figures 11 and 12 present the morphologies of UT, CT7, CT20, BT7, and BT20 after sliding at the speeds of 0.6 and 1.0 m/s, respectively. Similar features as observed for 0.2 m/s could also be seen at the speeds of 0.6 and 1.0 m/s, as evident from a comparison of Figs. 10(a), 11(a), and 12(a) for the untextured surface. The worn particles, in this case, remain present on the contact surface and cause abrasion and adhesion as the speed increases. However, the surface appears to be covered by a compacted layer probably of oxide at 1.0 m/s, which might have inhibited the metal–metal contact and reduced the friction coefficient by providing junctions of low shear strength as seen from Fig. 8. The textured surfaces show the presence of dimples either filled completely (CT7 and BT7) or partially (CT20 and BT20) with wear debris at a speed of 0.6 m/s. Oxidation processes at contacts are investigated, which are treated in a dry sliding by EDS (energy-dispersive X-ray spectroscopy). The elemental analysis obtained by EDS revealed the presence of iron and trace of oxygen on the surface and within the micro-dimples (Fig. 13). This suggests the presence of an oxide layer due to increased frictional heating caused by increased speed. Worn particles from the margin turnup of dimples are also added to the surface and accelerate abrasive wear before they are trapped in the cavities. SEM micrographs of CT7 and BT7 at a speed of 0.6 m/s and of all at 1.0 m/s show the presence of small patches of debris with an increase in speed (Figs. 11 and 12). The wear track shows some scratches that are oriented in the sliding direction. These surface features can be explained by abrasion wear, coupled with the oxidation phenomenon. In fact, oxide layers with high-mechanical properties form as a third body and give rise to wear of the disk at some positions.

However, at the highest speed of 1.0 m/s used in the current study, all the textured specimens are observed to be filled to the extent that dimples are not visible except for CT20. The bulge on the brim of the micro-dimple is also found to have disappeared completely.

The optical 3D profilometry of BT20 tested at 1 m/s is shown in Fig. 14. Before the test, the dimple has a certain average depth of about 8–10 μm , as can also be seen in the color bar. The high spots around the micropore are bulges on the brim. After the test, there is almost no evidence of the dimple. A worn track can be observed in the same region. Also, traces of abrasive wear are shown in Fig. 14(b).

The observed friction and wear behavior for the untextured steel may be explained on the basis of the adhesion between disk and counterface steel pin followed by generation of wear debris due to relative motion. The debris either gets trapped between the sliding surfaces or may get ejected from the interface due to centrifugal forces. The debris trapped between

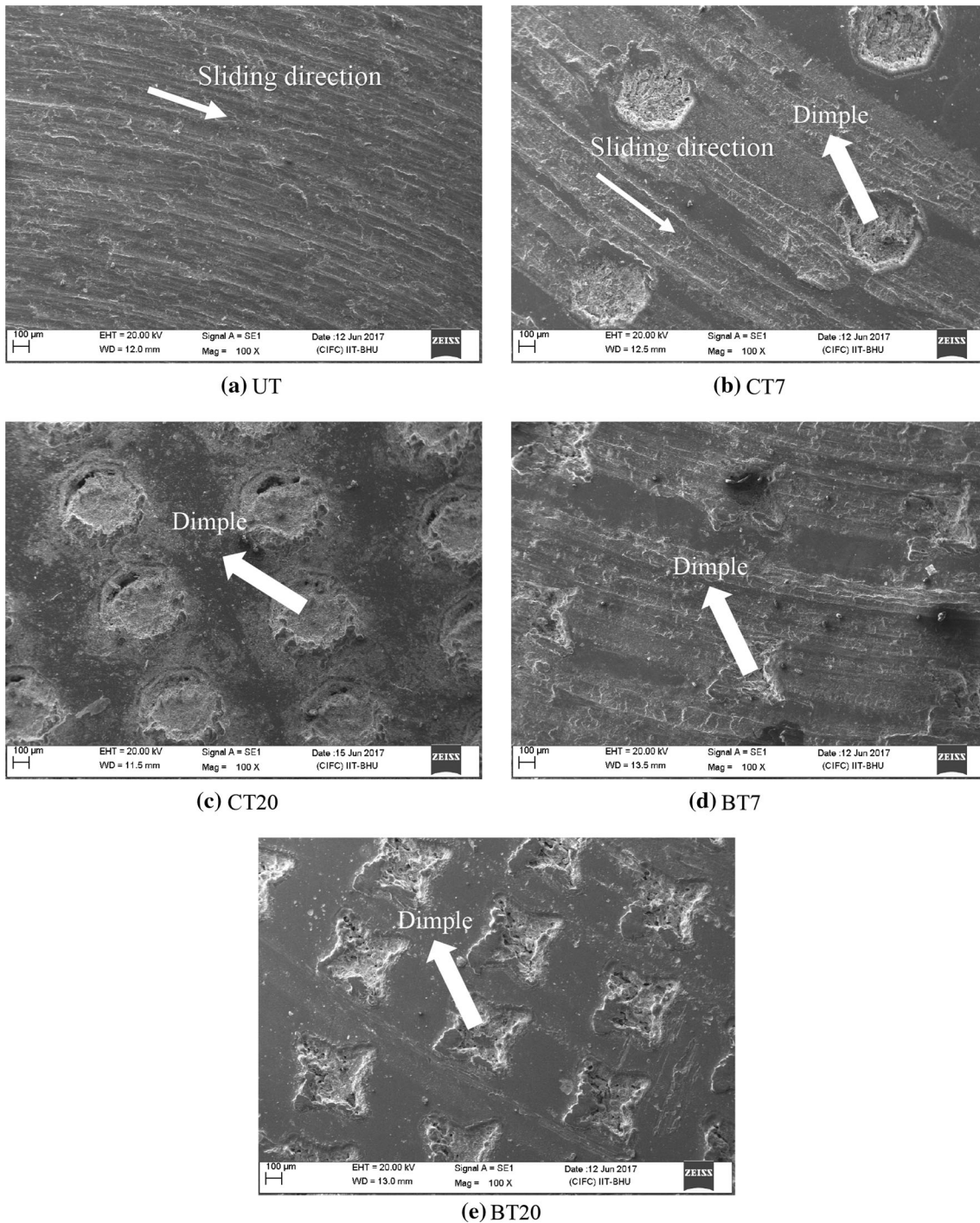


Fig. 10 Scanning electron micrographs of worn surface of specimens after sliding under the dry condition at 15 N constant load at 0.2 m/s

the surface may form a compacted layer on the sliding surface and results in a reduction in both friction and wear if that gets oxidized during continued rubbing by providing low-shear-strength junctions at the interface and protecting the underlying surface from direct metal to metal contact, as reported earlier also (Ref 25). The increase in friction and wear in UT steel from 0.2 m/s to 0.6 m/s may be attributed to the formation of more

number of wear particles due to larger number of interactions per unit time and more particles seem to have ejected as there is hardly any presence of transfer layer of the surface of this steel as observed in Fig. 11(a). However, the transfer layer containing oxide particles is expected to get compacted due to increased frictional heating caused by the increased speed, which provides an effective cover to the underlying substrate

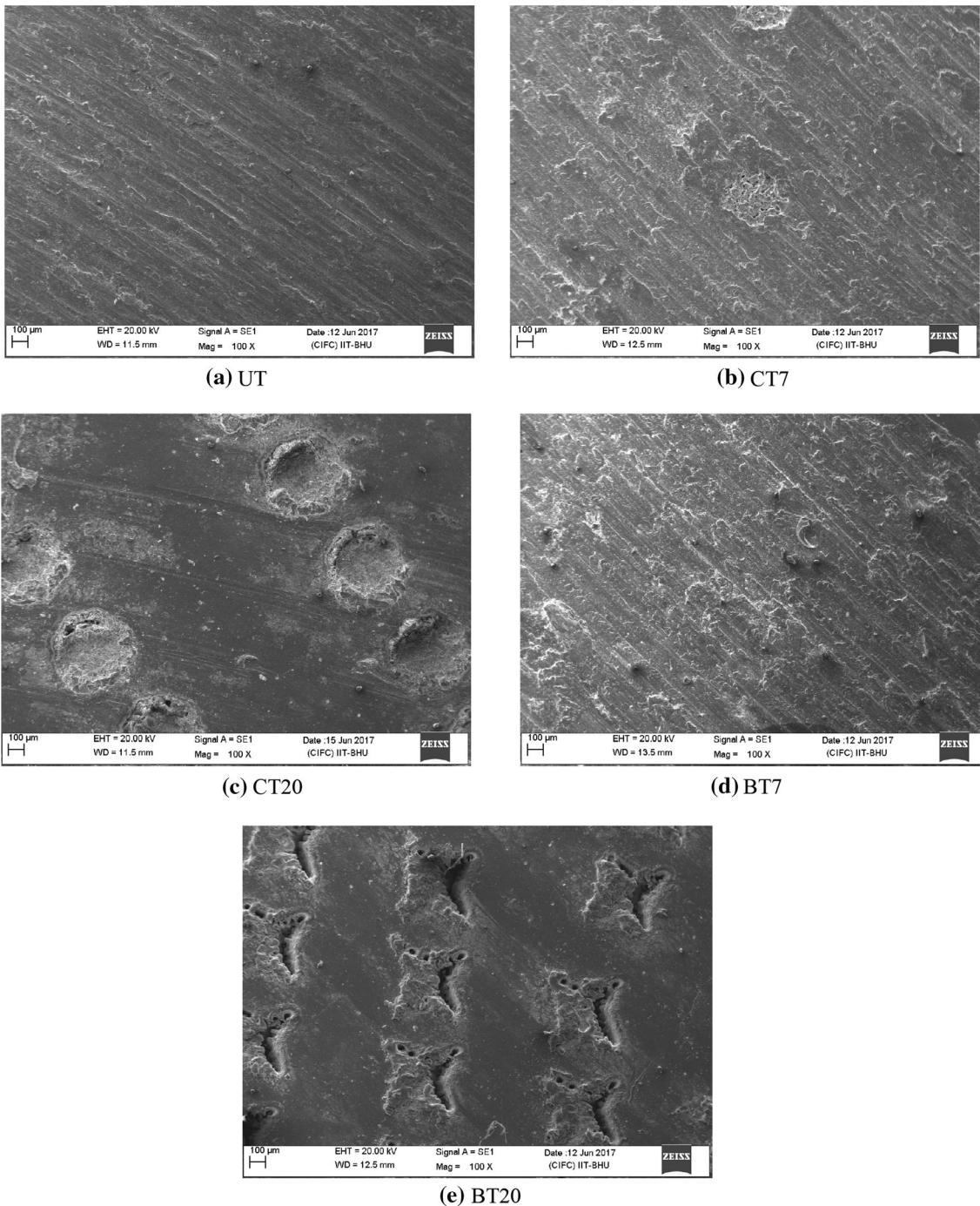


Fig. 11 Scanning electron micrographs of worn surface of specimens after sliding under the dry condition at 15 N constant load at 0.6 m/s

and reduces direct metal–metal contact leading to reduced friction and wear as reported earlier other researchers (Ref 25). As far as textured steels are concerned, the dimples are able to trap the wear debris particles, resulting in a reduced wear rate in comparison with untextured steel. At the lowest speed of 0.2 m/s, the friction coefficient is observed to decrease from UT to CT20 before increasing for BT20, as shown in Fig. 7, whereas the friction is found to decrease continuously from CT7 to

BT20 at the highest speed. The BT20 has the lowest friction coefficient of friction at relatively higher speeds of 0.6 m/s and 1.0 m/s, whereas, at the lowest speed, the friction is lowest for CT20 and BT7. At low speed of 0.2 m/s, pin moves in contact with the disk, as speed increases to 0.6 m/s bulges on the brim of dimples and at contact wears out, which gives the rise in coefficient of friction. As the edges are clear, these worn-out particles fill the cavity and result in a drop in the coefficient of

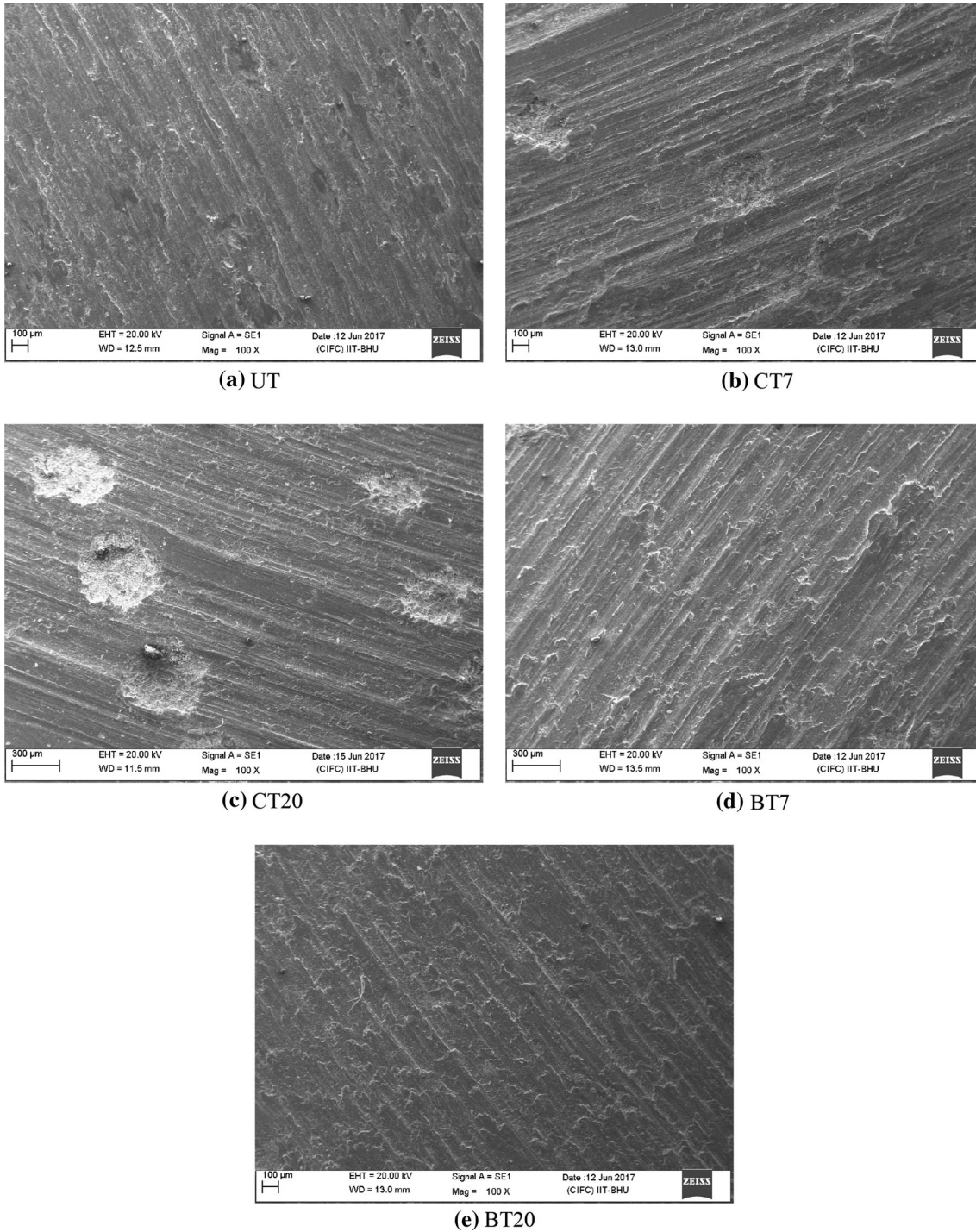


Fig. 12 Scanning electron micrographs of worn surface of specimens after sliding under the dry condition at 15 N constant load at 1.0 m/s

friction at 1 m/s. A relatively lower coefficient of friction for CT 20 and BT7 at a speed of 0.2 m/s may be explained on the basis of the features present on SEM micrographs presented in Fig. 10(c and d) which indicates the filling of dimples by the wear debris leading to the absence of any loose debris particles which might have caused abrasion. A reduced coefficient of

friction for CT20, BT7, and BT20 corresponding to a speed of 1 m/s may be attributed to the substantial unfilling of dimples, as reflected in Fig. 12(c) for CT20 and complete filling of dimples for BT7 and BT20 without any visible dimples, as seen from Fig. 12(d and e). This may have given rise to a smooth running as there was no loose debris available at the interface to

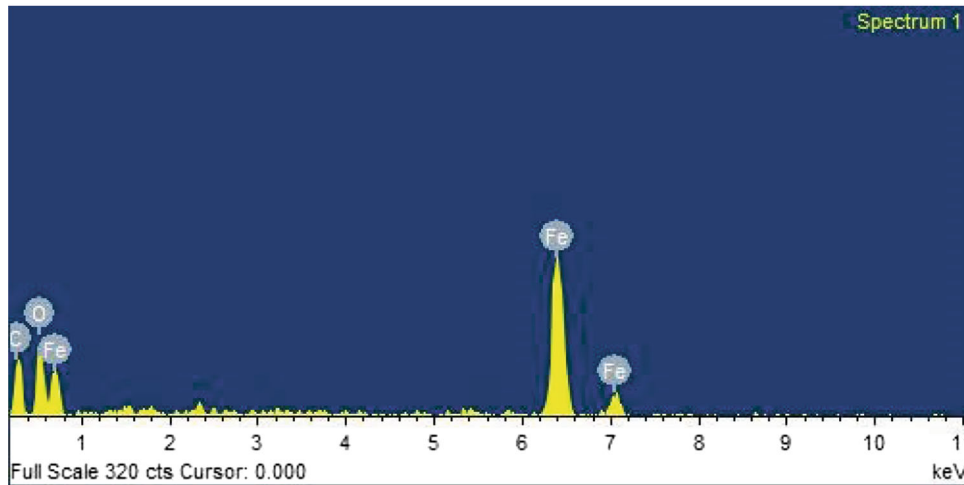
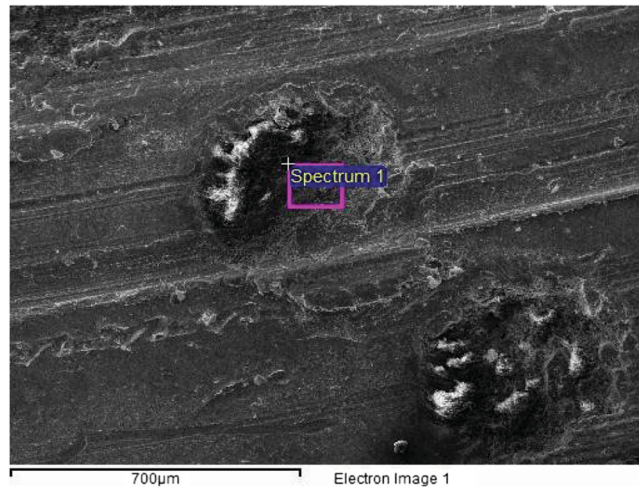


Fig. 13 SEM-EDS of worn surface of CT20 after sliding under dry condition at 15 N constant load at 1.0 m/s

cause abrasion, resulting in a decrease in coefficient of friction. The other factor contributing to this behavior may be the presence of a compact layer of oxide caused by frictional heating, which might have provided low-shearing junctions and hence a reduced coefficient of friction. The wear rate is found to be almost the same for CT7, CT20, and BT7 at speeds of 0.2 and 1.0 m/s, but BT20 has the lowest rate at 1.0 m/s, whereas it increases slightly for 0.2 m/s. The observed behavior may be attributed to the effectiveness of dimples in trapping the wear particles, which can be judged by an examination of worn surfaces of textured steels shown in Figs. 10, 11, and 12, where dimples appear to be filled to different extents depending on the test speed, shape, and density of dimples. At a relatively lower speed of 0.2 m/s, the dimples are partially filled due to less generation of loose wear debris, and hence, the wear is less than observed at other speeds. As the generation of wear particles is increased with increasing speed, the dimples get completely filled (Fig. 12b–e), and the remaining debris is not able to get trapped and get ejected as loose particles, thus increasing the

rate of wear. However, with a further increase in speed to 1.0 m/s, the wear rate is found to decrease again despite the filling of dimples. Under this condition, the untapped debris particles appear to have got compacted due to increased friction heating at the interface and form a compacted transfer layer (Fig. 12b–e), providing the protective cover to the underlying substrate to a varying extent leading to lower friction and wear.

A comparison of the friction and wear performance of circular and bi-triangular shape reflects that the bi-triangular shape is more effective in reducing both the friction and wear and that too with a relatively lower density of dimples as evident from Fig. 7 and 8, which shows either the same coefficient of friction for CT20 and BT7 or a reduced one for BT7 than CT20 depending on sliding speed. However, BT20 having bi-triangular dimples with 20% density has shown the optimum performance under the speeds and load used in the present study conducted under dry contact. Nonetheless, more studies need to be carried out to explore the optimum shape and density for dry as well as lubricated conditions.

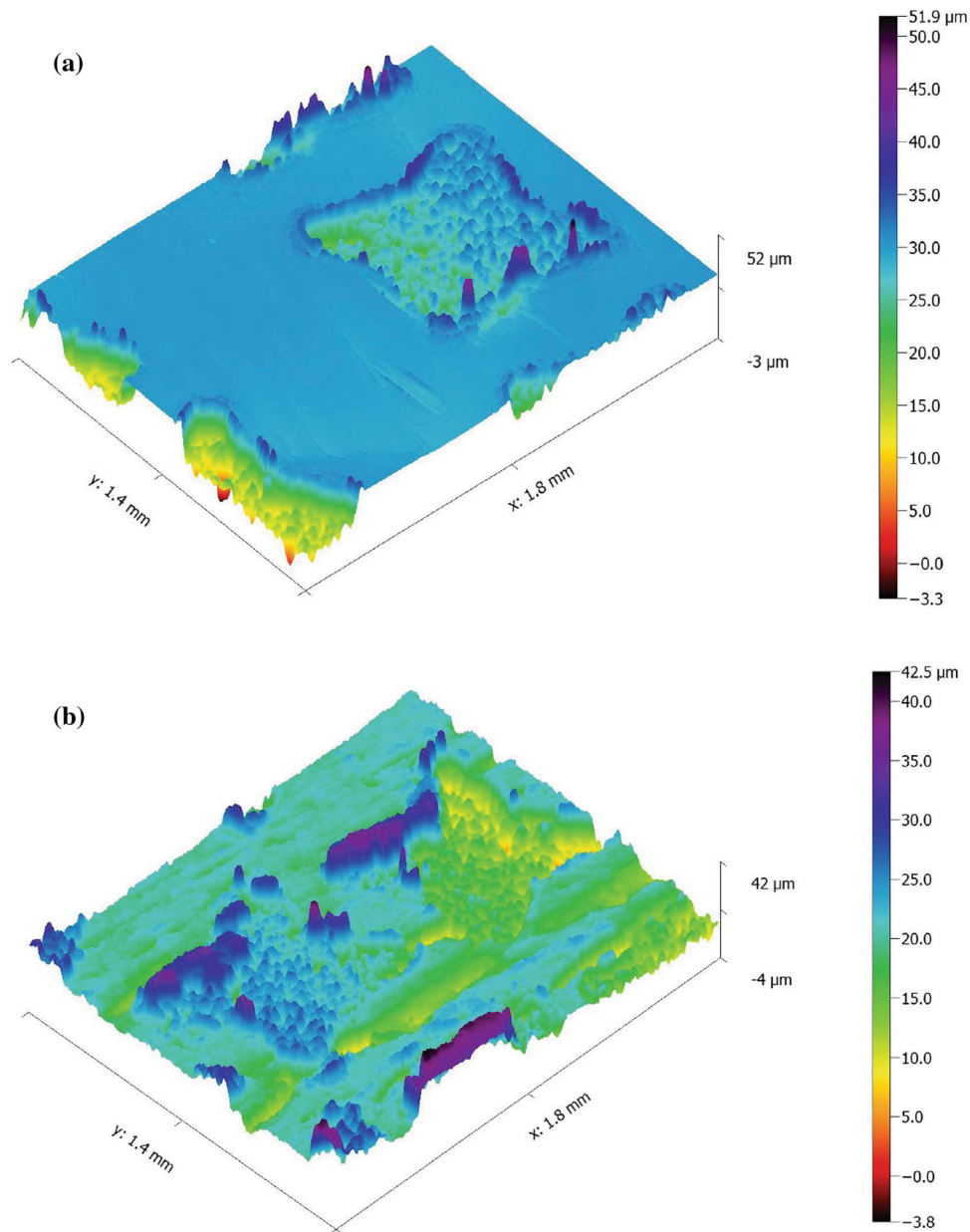


Fig. 14 Optical 3D profilometry of disk surfaces before (a) and after (b) the test

4. Conclusions

The present study on the effect of laser texturing on the dry sliding performance of bearing steel has led to the following salient conclusions.

1. An effective number of microcavities in the contact zone for the spiral array are relatively higher than in the case of a radial pattern. This increases the entrapment of a larger number of wear particles.
2. An increase in density of the dimples from 7 to 20% increases more entrapment possibility of wear debris and hence reduction in wear. However, once the cavity is filled, the texture effect is no more present.
3. Bi-triangular shape with relatively lower dimple density has been found to be more effective in comparison to the circular shape in reducing both the friction and wear. Bi-

triangular dimples with 20% density have shown the optimum performance under the conditions used in the present work.

4. In dry conditions, the coefficient of friction sliding pair with a textured sample is less than untextured one.

References

1. C. Gachot, A. Rosenkranz, S.M. Hsu, and H.L. Costa, Critical Assessment of Surface Texturing for Friction and Wear Improvement, *Wear*, 2017, **372–373**, p 21–41
2. I. Etsion, State of the Art in Laser Surface Texturing, in *Proceedings of ESDA04 7th Biennial Conference on Engineering Systems Design and Analysis*, (Manchester, United Kingdom, July 19–22, 2004)

3. B. Olofinjana, Effect of Laser Surface Texturing (LST) on Tribochemical Films Dynamics and Friction and Wear Performance, *Wear*, 2015, **332**, p 1225–1230
4. I. Etsion, Modelling of Surface Texturing in Hydrodynamic Lubrication, *Friction*, 2013, **1**(3), p 195–209
5. D.Z. Segu and P. Hwang, Friction Control by Multi-Shape Textured Surface Under Pin-on-Disc Test, *Tribol. Int.*, 2015, **91**, p 111–117
6. S.S. Perry and W.T. Tysoe, Frontiers of Fundamental Tribological Research, *Tribol. Lett.*, 2005, **19**(3), p 151–161
7. H.L. Costa, I.M. Hutchings, Lubricated Sliding Wear of Textured Surfaces, in *Proceedings of WTC III*, 2005
8. H. Zhang, A Mixed Lubrication Model for Studying Tribological Behaviours of Surface Texturing, *Tribol. Int.*, 2016, **93**(2), p 583–592
9. S. Wos, W. Koszela, and P. Pawlus, Determination of Oil Demand for Textured Surfaces Under Conformal Contact Conditions, *Tribol. Int.*, 2015, **93**, p 602–613
10. A. Borghi, Tribological Effects of Surface Texturing on Nitriding Steel for High-Performance Engine Applications, *Wear*, 2008, **265**, p 7–8
11. Y.G. Schneider, Formation of Surfaces with Uniform Micropatterns on Precision Machine and Instruments Parts, *Precis. Eng.*, 1984, **6**, p 219–225
12. U. Pettersson and S. Jacobson, Tribological Texturing of Steel Surfaces with a Novel Diamond Embossing Tool Technique, *Tribol. Int.*, 2005, **39**(7), p 695–700
13. X. Wang, K. Kato, K. Adachi, and K. Aizawa, Load Carrying Capacity Map for the Surface Texture Design of SiC Thrust Bearing Sliding in Water, *Tribol. Int.*, 2003, **36**(3), p 189–197
14. M. Wakuda, Y. Yamauchi, S. Kanzaki, and Y. Yasuda, Effect of Surface Texturing on Friction Reduction Between Ceramic and Steel Materials Under Lubricated Sliding Contact, *Wear*, 2003, **254**, p 356–363
15. U. Pettersson and S. Jacobson, Influence of Surface Texture on Boundary Lubricated Sliding Contacts, *Tribol. Int.*, 2003, **36**, p 857–864
16. I. Etsion, State of the Art in Laser Surface Texturing, *J. Tribol.*, 2005, **127**, p 248–253
17. M. Maillat, H.E. Hintermann, *Proceedings of the 5th International Congress on Tribology, Eurotrib 89*, (Helsinki, 1989), vol. 3, p. 16
18. A. Blatter, M. Maillat, S.M. Pimenov, G.A. Shafeev, A.V. Simakin, and E.N. Loubnin, Lubricated Sliding Performance of Laser-Patterned Sapphire, *Wear*, 1999, **232**, p 226–230
19. I. Etsion, State of the art in laser surface texturing, in *Proceedings of ESDA04, 7th Biennial Conference on Engineering Systems Design and Analysis*, 2004
20. D. Patel, V.K. Jain, and J. Ramkumar, Surface Texturing for Inducing Hydrophobicity, *Directions*, 2015, **15**(1), p 46–53
21. E. Tomanik, Modelling the Hydrodynamic Support of Cylinder Bore and Piston Rings with Laser Textured Surfaces, *Tribol. Int.*, 2013, **59**, p 90–96
22. Olhydraulik und Pneumatik 46 (2002). [17] G. Dumitru, V. Romano, H.P. Weber, H. Haefke, Y.E. Gerbig, Pflugger, Laser Micro-Structuring of Steel Surfaces for Tribological Applications. *Appl. Phys.*, A 70, 485–487 (2000)
23. T. Sugihara and T. Enomoto, Improving Anti-Adhesion in Aluminum Alloy Cutting by Micro Stripe Texture, *Precis. Eng.*, 2012, **36**, p 229–237
24. A. Rosenkranz, P.G. Grützmacher, C. Gachot, and H.L. Costa, Surface Texturing in Machine Elements—A Critical Discussion for Rolling and Sliding Contacts, *Adv. Eng. Mater.*, 2019, **21**(8), p 1900194
25. R. Tyagi, S.K. Nath, and S. Ray, Effect of martensite content on friction and oxidative wear behavior of 042 pct carbon dual phase steel, *Met. Metall. Trans. A*, 2002, **33**, p 3388–3479

Publisher's Note Springer Nature remains neutral with regard to jurisdictional claims in published maps and institutional affiliations.